13th International Symposium on Turbulence and Shear Flow Phenomena (TSFP13)
Montreal, Canada, June 25–28, 2024

AN EXPERIMENTAL INVESTIGATION OF TANGENTIAL AND RADIAL VELOCITY STATISTICS OF A ROTATING DISK BOUNDARY LAYER

Mohammadreza Mollaei
Department of Mechanical Engineering
University of Melbourne
Parkville, Victoria 3010, Australia
mmollaei@student.unimelb.edu.au

Jimmy Philip
Department of Mechanical Engineering
University of Melbourne
Parkville, Victoria 3010, Australia
jimmyp@unimelb.edu.au

Joseph C. Klewicki
Department of Mechanical Engineering
University of Melbourne
Parkville, Victoria 3010, Australia
klewicki@unimelb.edu.au

ABSTRACT

Turbulence statistics of the 3D boundary layer flow over a confined-domain rotating disk are investigated at varying Reynolds numbers. Using a two-view molecular tagging velocimetry system, instantaneous tangential and radial velocity profiles are obtained simultaneously as a function of the wall-normal direction. Mean and rms velocity profiles, and the crossflow-induced Reynolds shear stress are examined, and a comparative assessment is made between these turbulence statistics for the rotating disk boundary layer and available data of the 2D canonical flow over a flat plate. The well-known log-law equation with $\kappa = 0.384$ and $B = 4.17$ represents the inner-scaled mean tangential velocity profile close to the edge of the boundary layer at all Reynolds numbers with a negligible wake area for this 3D turbulent flow. The rms values for both tangential and radial velocities remain smaller than the DNS results of the 2D boundary layer. The Reynolds stress correlation coefficient has a maximum of around $0.3 \sim 0.35$ representing the influence of the crossflow component on the turbulence structure of the rotating disk boundary layer. In contrast, the contribution of the corresponding Reynolds stress component is identically zero in the canonical zero-pressure-gradient boundary layer.

INTRODUCTION

Three-dimensional (3D) crossflow effects within wall flows emerge while employing rotating surfaces, such as in gas turbine engines, separation processes, computer hard drives, and chemical vapour deposition processes (Imayama, 2012). In addition, cross-flow effects are important in investigating flow over the swept wings of aircraft (Lin and Reed, 1993), and while applying drag reduction strategies (Quadrio, 2011).

For the fundamental study of 3D wall flows, the rotating disk boundary layer (RDBL) flow provides a useful context, as it has an exact similarity solution to the Navier-Stokes equations for the laminar flow, introduced by von Kármán (1921), and this flow is 3D from its inception. Thus, in this respect, the RDBL constitutes a canonical 3D wall flow. This flow has been the subject of extensive examinations in stability analysis and transition to turbulence studies (e.g. Imayama, 2012). However, relatively few works have explored fully developed turbulent boundary layer flow over a rotating disk, especially at high Reynolds numbers.

In this flow, the rotation of the disk drives both the tangentially oriented boundary layer and the radially outward crossflow. Due to the conservation of mass and the pumping effect of the disk, the wallward flow converts into the radial outflow. For laminar flow, von Kármán (1921) obtained a 3D similarity solution to the steady Navier-Stokes equations assuming an infinite disk rotating with constant angular velocity within a stationary fluid. Two types of Reynolds numbers are typically defined for this flow; the first one is usually used for laminar flow and stability analyses as $Re = r(\Omega/\nu)^{1/2}$ where r is the local radius of the disk, Ω is the angular velocity of the disk, and ν is the kinematic viscosity of the fluid. Imayama (2012) suggested that a fully developed turbulent flow over an infinite rotating disk can be observed for Reynolds numbers greater than 650. Friction Reynolds number (δ^+) is utilised in transitional and turbulent investigations. Here, $\delta^+ = U_{\theta_\tau}\delta/\nu$, where δ represents the local thickness of the boundary layer and U_{θ_τ} is the tangential friction velocity, which is defined as $U_{\theta_\tau} = \sqrt{\nu \frac{dU_\theta}{dz}|_{z=0}}$, with z as the wall-normal distance.

To study this flow, a non-intrusive technique, molecular tagging velocimetry (MTV), is utilised to measure tangential and radial velocity components. The focus of the current study is to provide high-resolution measurements for turbulent RDBL flow over a substantial Reynolds number range using a two-view MTV system, as shown in Figure 1. Thus, through these experiments, spatially resolved wall-normal instantaneous velocity profiles are simultaneously obtained in the radial and tangential directions. We aim to leverage the instantaneous radial and azimuthal velocity profiles to reveal the role of crossflow in the turbulent RDBL structure. Present measurements enable the ability to clarify the crossflow-induced correlation structure of the fully developed turbulent flow, as compared to a canonical 2D turbulent boundary layer (2DTBL), and allow us to compare and contrast both mean and turbulence statistics of high Reynolds RDBL with a

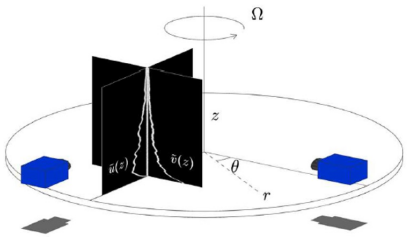

Figure 1. Arrangement of two orthogonally placed cameras to obtain azimuthal and radial instantaneous velocity profiles.

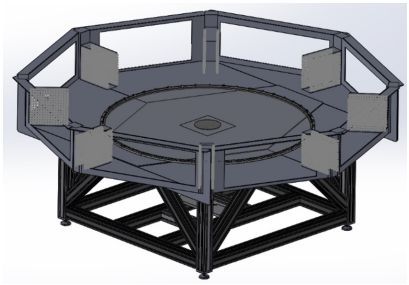

Figure 2. An isometric view of the rotating disk facility.

zero-pressure-gradient (ZPG) boundary layer.

EXPERIMENT

We first describe the MTV measurement technique and then present details of the experimental setup. The MTV method leverages the phosphorescence effect lasting several milliseconds produced by water-soluble supramolecular complexes. The triplex used in the present experiments is 1-BrNP.Mβ-CD.ROH which contains 1-Bromonaphthalene (1-BrNP), maltosyl-β-cyclodextrin (Mβ-CD), and cyclohexanol as alcohol (ROH). In this approach, phosphorescent molecules are excited using a pulsed laser, and tagged molecules are used as a tracer to measure flow properties, such as temperature and velocity (Hu and Koochesfahani, 2006). In this study, a pulsed UV Excimer laser with a wavelength of 308 nm is used to tag phosphorescent molecules with a frequency of up to 15 Hz. The images are taken by two orthogonally placed pco.dicam C1 intensified 16-bit sCMOS cameras with an image array of 1504 × 1304 pixels (c.f. Figure 1).

The experiments are carried out in a custom-made rotating disk facility illustrated in Figure 2 that, to the authors' knowledge, is perhaps the largest of its kind with a diameter of 1.6 m, i.e. 60% larger than the one employed in previous air-based hot-wire studies (e.g. Itoh and Hasegawa, 1992; and Littell and Eaton, 1991). The edge of the rotating disk is 0.5 m from the side windows. The disk is made of polished glass and is centred in a large octagonal tank made of G10 fibreglass. The surface of the glass disk is painted black to remove the reflection of the MTV line from the disk surface. A circular perforated plate is used around the disk to break up the momentum of the flow and to create an infinite-domain approximation for the flow above the disk. Furthermore, double-sided mesh frames have been installed at all eight corners of the tank to reduce the rotation of the flow outside the boundary layer and hence minimise secondary flow effects. The disk is coupled to a shaft from below and is rotated via a belt that connects the shaft to a three-phase induction motor. The motor is controlled with a variable frequency drive that adjusts the disk rpm with a resolution of 0.02 rpm by changing the motor frequency.

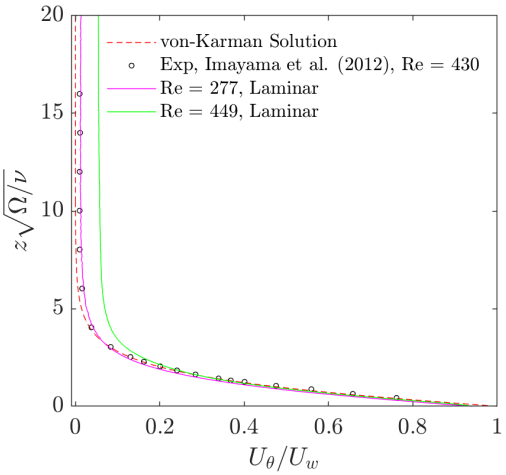

Figure 3. Normalised mean tangential velocity profiles in the laminar regime.

RESULTS

The UV laser beam enters the MTV solution from the top and tags a straight line perpendicular to the disk within the solution. The instantaneous radial and tangential velocities can be obtained by taking two successive images, one of the undeformed line upon excitation, and another of the deformed line due to the fluid motion. We can vary the Reynolds number by changing either the location where the laser beam touches the disk (i.e. r) or the disk rpm.

The mean tangential and radial velocity distributions of the laminar flow normalised by the local wall velocity (i.e. $U_w = r \times \Omega$) versus the laminar normalised distance from the wall (i.e. $z\sqrt{\Omega/\nu}$) are plotted in Figures 3 and 4, respectively. The measurements are conducted at $r = 420$ mm for two Reynolds numbers within the range of laminar flow ($Re \lesssim 500$). Unlike von Kármán's similarity solution for the laminar flow over an infinite rotating disk, both tangential and radial velocity components approach small but non-zero values outside the boundary layer. This highlights the main difference between the infinite and the present confined-geometry rotating disks. In this regard, Mory and Spohn (1992) also reported the presence of a non-zero rotation outside the boundary layer of a confined-domain rotating disk at $r/R = 0.5$.

The secondary flow in the confined-geometry configuration affects the flow statistics. It can be seen in Figure 3 wherein the tangential velocity closely matches the similarity solution profile in the inner part of the laminar boundary layer then starts deviating from the exact solution for $U_\theta/U_w < 0.2$ and approaches a small but non-zero value outside the boundary layer. The tangential velocity data at $Re = 277$ is in good agreement with the hot-wire data acquired by Imayama (2012).

In contrast to the tangential velocity, the secondary flow apparently influences the radial component across the entire boundary layer, as shown in Figure 4. Here, the mean radial velocity magnitude is always larger than that of the similarity solution. The departure from the similarity solution was recorded by Littell and Eaton (1991) and Digre (2015) as well while measuring mean radial velocity on a rotating disk. The normalised location of the peak in the radial velocity profiles, however, matches well with the exact solution and is nearly constant with increasing Reynolds number.

The characteristics of the fully turbulent flow for both the tangential and radial velocity components are investigated at $r = 750$ mm (i.e. $r/R = 0.94$) for varying rpm. Here, we ex-

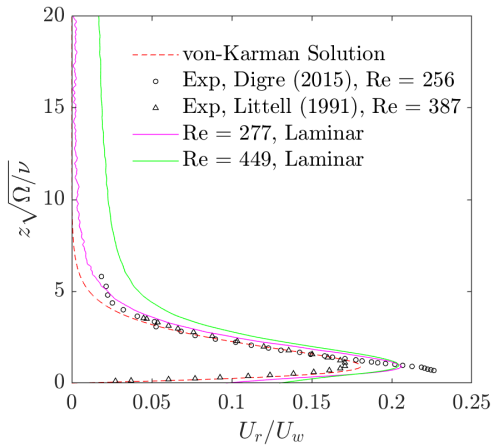

Figure 4. Normalised mean radial velocity profiles in the laminar regime.

amine the mean and rms velocity profiles, and Reynolds stress derived from the tangential and radial velocity fluctuations. A comparative assessment is made between these characteristics for the RDTBL and available DNS data of the 2DTBL over a flat plate at ZPG from Schlatter and Örlü (2010). It should be noted that two sets of DNS data of the 2DTBL are used for comparison; one with an analogous coefficient of friction ($C_f = 0.003539$ at $\delta^+ = 671$ for 2DTBL corresponding to $C_f = 0.003537$ at $\delta^+ = 1870$ for 3D RDTBL where C_f is defined as $C_f = \frac{\tau_{w_\theta}}{\frac{1}{2}\rho U_w{}^2}$), and another one with a comparative friction Reynold number at $\delta^+ = 1272$ which is also the highest Reynolds number investigated by Schlatter and Örlü (2010).

Details of the investigated cases are presented in Table 1. Henceforth, the colours of the plots are the same as presented in Table 1. In this context, the boundary layer thickness (δ) is where $U_w - (U_\theta - U_\infty) \approx 0.99U_w$ where U_∞ is the mean tangential velocity outside the boundary layer which is very close to zero. The variations of some of the flow parameters with Reynolds number are demonstrated in Figure 5, derived from the tangential velocity profiles in the turbulent regime. The shape factor (H) is stated as the ratio of displacement thickness δ^* to momentum thickness θ defined as $\delta^* = \int_0^\delta \frac{U_\theta(z)}{U_w}\,dz$ and $\theta = \int_0^\delta (1 - \frac{U_\theta(z)}{U_w})\frac{U_\theta(z)}{U_w}\,dz$, respectively.

Table 1. Summary of present experiments at $r = 750$ mm.

	Re	δ^+	δ	δ^*	θ	U_{θ_τ}	U_w
			$[mm]$	$[mm]$	$[mm]$	$[m/s]$	[m/s]
–	812	1200	30.9	3.5	2.7	0.0421	1.01
–	1047	1870	30.4	3.3	2.6	0.0665	1.69
–	1161	2230	30.0	3.1	2.5	0.0805	2.07
–	1265	2610	30.1	3.1	2.5	0.0938	2.46
–	1348	2840	29.1	2.9	2.4	0.1055	2.79

By comparing the values of δ at $r = 420$ mm (not presented herein) and 750 mm, we conclude that the turbulent

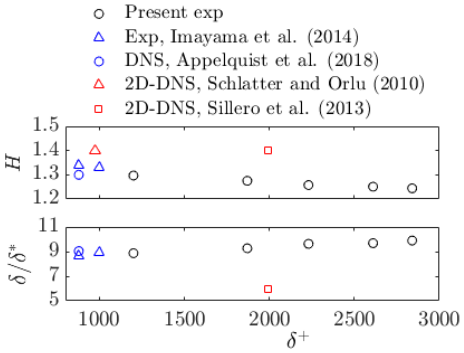

Figure 5. Flow parameters vs. friction Reynolds number.

boundary layer thickness increases in the radial direction even though it is independent of the radial location in the analytical solution of the laminar flow. It appears, however, to exhibit a minor decrease with Reynolds number at $r = 750$ mm. Current measurements also indicate a slight decrease in displacement thickness and momentum thickness values with increasing Reynolds number. The average shape factor equals $H = 1.27$ which is closer to the empirical value 1.33 reported by Imayama *et al.* (2014) for the RDTBL at $\delta^+ = 999$ and is lower than the approximate value 1.4 obtained for the 2DTBL flow over a flat plate at comparable Reynolds numbers (Schlatter and Örlü, 2010; Sillero *et al.*, 2013). Appelquist *et al.* (2018) also found smaller shape factor values compared to the 2DTBL from the DNS study of an infinite domain RDTBL. In the present study, the ratio of δ/δ^* is 8.9 at $\delta^+ = 1200$ which is in good agreement with the value of 9 reported by Imayama *et al.* (2014). This ratio is, however, larger than 5.6 found for the 2DTBL flow (Schlatter and Örlü, 2010). Both a smaller shape factor and larger δ/δ^* ratio are indicators of a fuller velocity profile in RDTBL compared to the 2D ZPG flow (Imayama *et al.*, 2014).

The mean tangential and radial velocity distributions at different Reynolds numbers normalised by the local disk velocity are shown in Figure 6. Except for the plots at $Re = 812$, it is seen that the mean velocity profiles nearly merge in Figures 6 (a) and (b). It is noted here that each velocity profile consisted of 1304 data points from equally-spaced pixels with a millimetre-to-pixel ratio of 0.0323 and 0.0496 in the tangential and radial directions, respectively.

The accuracy of the measured velocities near the wall is adversely affected by some factors such as disk wobble, which is more severe at lower rpms ($\sim$ 1.5 mm per revolution at $\delta^+ = 1200$), spatial averaging, and laser beam's attenuation due to penetration through the MTV solution. Owing to the difficulty in measurement close to the wall, U_θ/U_w is not exactly unity on the wall and the discrepancy from this limit increases with Reynolds number as shown in Figure 6 (a). A similar trend is seen for the radial velocity in Figure 6 (b), where U_r/U_w increasingly departs from zero as Reynolds number increases. In contrast to the velocity data acquired at $r = 420$ mm, tangential and radial velocities approach nearly zero outside the boundary layer for all cases at $r = 750$ mm. This indicates that the flow field is either not affected by the secondary flow or its influence is insignificant when compared to the larger disk velocity at this location.

Figure 7 shows the inner-normalised mean tangential velocity profiles at various friction Reynolds numbers. The results at $\delta^+ = 1200$ are compared to the hot-wire data of Itoh and Hasegawa (1992) at $\delta^+ \approx 1500$ and the DNS data of Appelquist *et al.* (2018) at $\delta^+ \approx 900$. Moreover, 2DTBL data

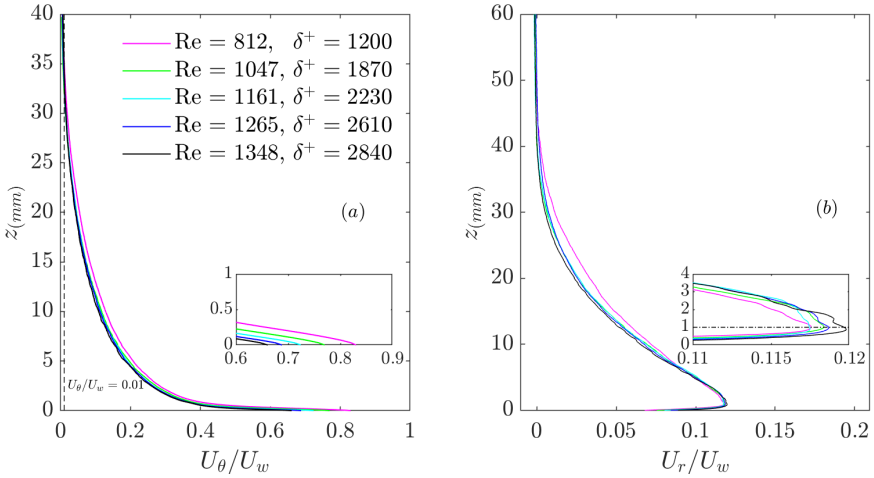

Figure 6. Mean tangential and radial velocities normalised by disk's local velocity vs. wall-normal distance.

from the DNS of Schlatter and Örlü (2010) is also included. It should be noted that the friction velocity herein has been extracted from the Clauser chart method (i.e. by assuming the log-law equation with $\kappa = 0.41$ and $B = 5$). This method is used since the mean velocity data within the viscous sublayer is not sufficiently reliable for directly measuring the friction velocity, especially at higher Reynolds numbers.

It can be seen that RDTBL and 2DTBL have similar trends in the inner part of the boundary layer even though data points within the viscous sublayer are missing in the present study due to the reasons discussed. In the outer part of the boundary layer, the situation is different. If we consider the collapse of the data on the well-known law of the wall for the 2DTBL (with $\kappa = 0.41$ and $B = 5$), as evidenced in Alfredsson *et al.* (2013) and Appelquist *et al.* (2018), a weak visible wake area is seen for the RDTBL flow but if we consider the log-law equation with $\kappa = 0.384$ and $B = 4.17$, it represents the inner-scaled mean velocity profile up to the edge of the boundary layer at nearly all Reynolds numbers with negligible wake area for this 3D turbulent flow as pointed out by other studies on the RDTBL (e.g. Itoh and Hasegawa, 1992; Imayama *et al.*, 2014; and Appelquist *et al.*, 2018). Digre (2015) suggested that the mean azimuthal velocity data of the RDTBL collapses well on the log-law with $\kappa = 0.384$ and $B = 4.33$ for the range of Reynolds numbers investigated. Moreover, Nagib *et al.* (2004) indicated that the mean streamwise velocity data of a 2D zero pressure gradient flow collapses very well on the logarithmic profile with $\kappa = 0.38$ and $B = 4.1$ for an extensive momentum Reynolds number range of $1000 < Re_\theta < 70000$.

Figure 8 depicts the inner-normalised mean radial velocity profiles at various Reynolds numbers. The mean radial velocities have been scaled using the tangential friction velocity as the radial friction velocity cannot be extracted directly from the present measurements. The results at $Re = 1047$ (green line) collapse well on the data from Itoh and Hasegawa (1992) at $Re = 1000$ and all velocity distributions follow the shape of the DNS data from Appelquist *et al.* (2018) at $Re = 669$. The accuracy of the measurements decreases within the viscous sublayer as observed for the tangential velocity as well.

Inner-normalised rms profiles of tangential and radial velocities are presented in Figures 9 and 10, respectively. The present rms profiles have a smaller amplitude than in the DNS data for both tangential and radial components. This observed difference primarily results from the spatial attenuation due to the spatial averaging effect of the MTV technique (Elsnab *et al.*, 2017). The attenuation can be nominally corrected by the method suggested by Lee *et al.* (2016). It can be observed that the corrected profiles at $\delta^+ = 1200$ are fairly consistent both qualitatively and quantitatively with that for the hot-wire corrected data acquired by Itoh and Hasegawa (1992). The corrected rms velocity values and the DNS results, for the RDTBL, remain lower than the DNS results obtained for the 2D flow over a flat plate across the boundary layer. Reporting the same observation for tangential rms velocity, Imayama *et al.* (2014) hypothesised that the smaller rms values stem from the presence of less influential large-scale motions in the outer part of the RDTBL flow that leave a weaker footprint on the near-wall structures compared to 2DTBL.

The distribution of Reynolds shear stress correlation coefficient defined as $\rho_{u_\theta u_r} = \frac{\overline{u_\theta u_r}}{u_{\theta_{rms}} u_{r_{rms}}}$ are shown for various Reynolds numbers in Figure 11. The shape of the Reynolds shear stress correlation coefficient plots is analogous to that of the DNS study with a negative minimum located around $z^+ = 5 \sim 10$ and a maximum in the outer part of the boundary layer. The change in the sign of the plots close to the wall is attributed to the change in the mean radial velocity gradient $\frac{\partial U_r}{\partial z}$ within this range (Itoh and Hasegawa, 1992). Even though the amplitude of the maximum Reynolds stress correlation coefficient appears to remain almost constant in Figure 11, the amplitude of its minimum is reduced with increasing Reynolds number. However, it is hypothesised to be due to the uncertainty of the measured fluctuations near the wall especially at higher Reynolds numbers.

It should be noted that $\rho_{u_\theta u_r}$ is a representative of turbulent momentum transport efficiency, whereas $\overline{u_\theta u_r}$ can be influenced by the existing fluctuation energy, i.e. rms of u_r and u_θ (Romero *et al.*, 2022). As shown in Figure 11, the Reynolds stress correlation coefficient has a maximum of around $0.3 \sim 0.35$ indicating a high level of turbulent momentum transport resulting from the crossflow fluctuations in the outer part of this 3D canonical boundary layer.

CONCLUSIONS

This work presents experimental results of the study of a 3D turbulent boundary layer over a rotating disk where water is used as the working fluid, and hence the domain is not infinite. To conduct fundamental studies of 3D wall flows, the rotating disk boundary layer is an appropriate case study. This flow offers an exact similarity solution to the Navier-Stokes equations for laminar flow, as introduced by von Kármán (1921), and is

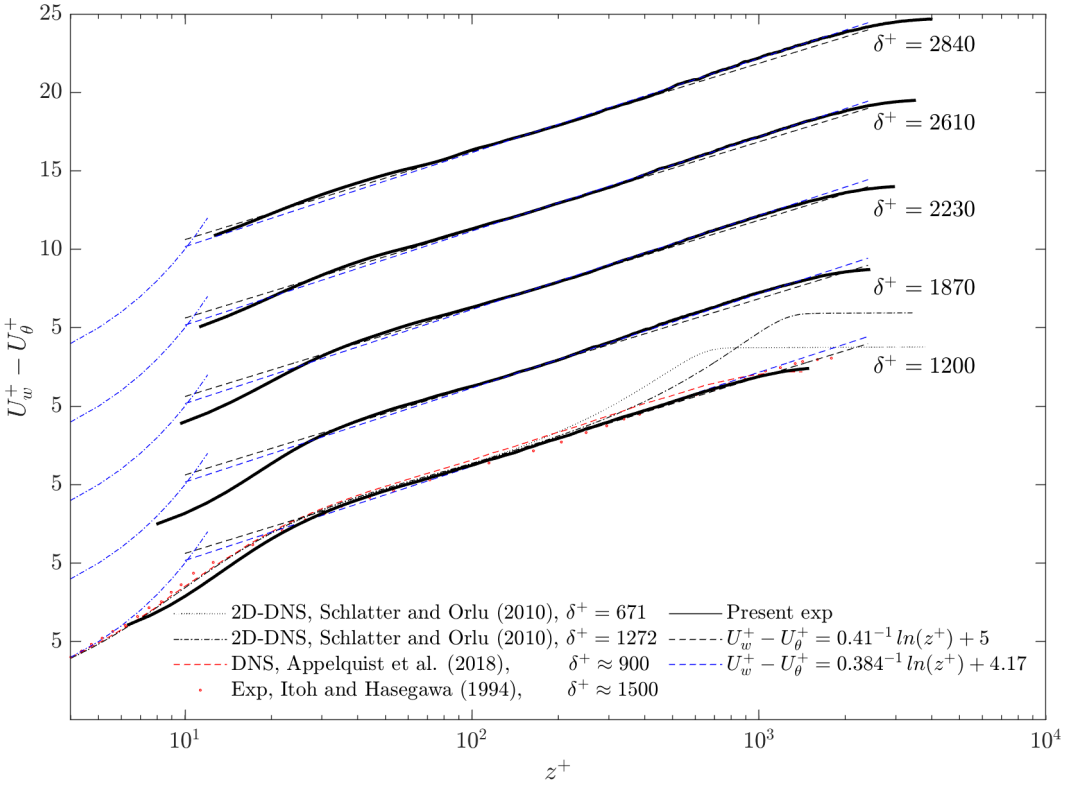

Figure 7. Inner-normalised mean tangential velocity profiles vs. viscous scaled distance to the wall. The plots of two successive δ^+ are shifted by 5 in the vertical direction.

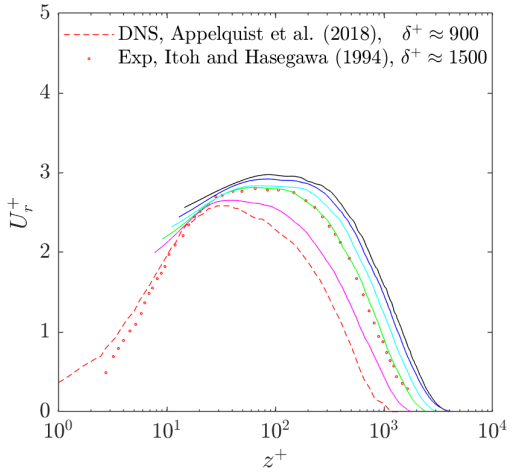

Figure 8. Inner-normalised mean radial velocity profiles.

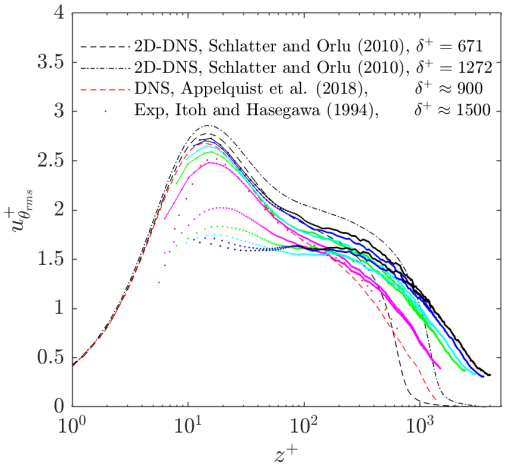

Figure 9. Inner-normalised tangential rms velocity profiles. Dots represent the measured values and solid lines represent corrected values using the method of Lee *et al.* (2016).

inherently 3D. The main results of this experimental study can be summarised as follows.

- Laminar velocity profiles match closely with von Kármán's similarity solution. However, both tangential and radial velocity components for the laminar flow approach small but non-zero values outside the boundary layer probably because of the confined domain which is also supported by Mory and Spohn (1992) who observed a non-zero rotation outside the boundary layer of a confined-domain rotating disk at $r/R = 0.5$.
- The physical location of the peak in the mean radial velocity profiles remains nearly constant at around 1 mm with increasing Reynolds number.
- The boundary layer thickness of the turbulent flow increases with r and slightly reduces with Ω at a fixed r, while it does not depend on the radial location in the analytical solution for the laminar flow.
- The present RDTBL appears to show a smaller shape factor value compared to the 2DTBL flow which is in agreement with the previous studies on the rotating disk flow.
- The law of the wall equation with $\kappa = 0.384$ and $B = 4.17$ well represents the inner-normalised mean tangential velocity profile up to the boundary layer's edge at all Reynolds numbers without a visible wake area for this 3D canonical wall flow.
- The rms profiles for both tangential and radial velocities remain below their counterparts in 2DTBL at similar fric-

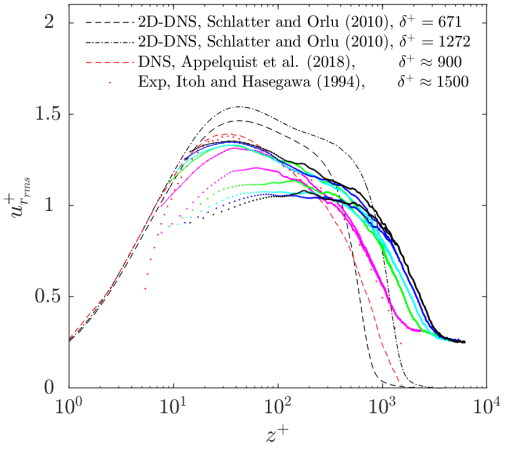

Figure 10. Inner-normalised radial rms velocity profiles. Dots represent the measured values and solid lines represent corrected values using the method of Lee *et al.* (2016).

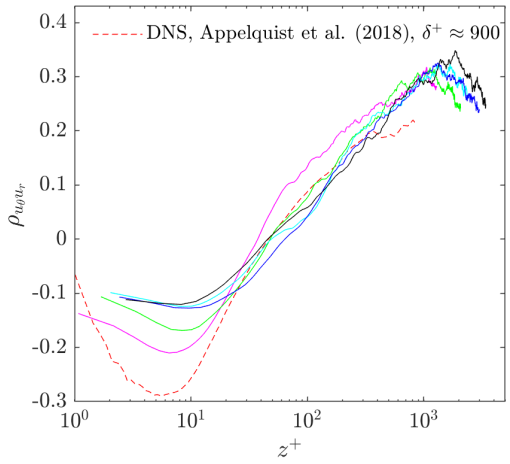

Figure 11. Inner-normalised distribution of Reynolds shear stress correlation coefficient.

tion Reynolds numbers even after correction.

- The Reynolds stress correlation coefficient has a maximum of around $0.3 \sim 0.35$ representing a high level of turbulent momentum transport due to the crossflow component in the RDTBL flow.

The apparent good quality of the present data and the available DNS and experimental findings allow us to take the next steps toward the aim of this study, which is measuring other Reynolds stress components involving wall-normal velocity fluctuations (u_z) using the Laser Doppler Velocimetry technique (LDV). Hence, conducting LDV experiments will shed more light on how the crossflow modifies the correlation structure of the fully developed turbulent flow compared to canonical 2D boundary layers.

ACKNOWLEDGEMENTS

This work was supported by the Australian Research Council under award number DP200101990.

REFERENCES

Alfredsson, P. H., Imayama, S., Lingwood, R. J., Örlü, R. and Segalini, A. 2013 Turbulent boundary layers over flat plates and rotating disks—the legacy of von kármán: A stockholm perspective. *Eur. J. Mech. B/Fluids* **40**, 17–29.

Appelquist, E., Schlatter, P., Alfredsson, P. H. and Lingwood, R. J. 2018 Turbulence in the rotating-disk boundary layer investigated through direct numerical simulations. *Eur. J. Mech. B/Fluids* **70**, 6–18.

Digre, D. 2015 The three-dimensional turbulent boundary layer on a rotating disk. Master's thesis, Embry-Riddle Aeronautical University. Department of Aerospace Engineering.

Elsnab, J. R., Monty, J. P., White, C. M., Koochesfahani, M. M. and Klewicki, J. C. 2017 Efficacy of single-component mtv to measure turbulent wall-flow velocity derivative profiles at high resolution. *Exp. Fluids* **58**, 1–11.

Hu, H. and Koochesfahani, M. M. 2006 Molecular tagging velocimetry and thermometry and its application to the wake of a heated circular cylinder. *Meas. Sci. Technol.* **17** (6), 1269.

Imayama, S. 2012 Experimental study of the rotating-disk boundary-layer flow. PhD thesis, KTH Royal Institute of Technology.

Imayama, S., Lingwood, R. J. and Alfredsson, P. H. 2014 The turbulent rotating-disk boundary layer. *Eur. J. Mech. B/Fluids* **48**, 245–253.

Itoh, M. and Hasegawa, I. 1992 Turbulent boundary layer on a rotating disk in an infinite quiescent fluid. *JSME Transactions* **58**, 98–105.

von Kármán, T. 1921 Über laminare und turbulente reibung. *ZAMM* **1** (4), 233–252.

Lee, J. H., Kevin, Monty, J. P. and Hutchins, N. 2016 Validating under-resolved turbulence intensities for piv experiments in canonical wall-bounded turbulence. *Exp. Fluids* **57**, 1–11.

Lin, R. S. and Reed, H. L. 1993 Effect of curvature on stationary crossflow instability of a three-dimensional boundary layer. *AIAA J.* **31** (9), 1611–1617.

Littell, H. S. and Eaton, J. K. 1991 Experimental investigation of the three-dimensional boundary layer on a rotating disk. In *Turbulent Shear Flows 8: Selected Papers from the Eighth International Symposium on Turbulent Shear Flows, Munich, Germany, September 9–11, 1991*, pp. 403–414. Springer.

Mory, M and Spohn, A 1992 Vortex flow generated by a rotating disc. In *Rotating fluids in geophysical and industrial applications*, pp. 301–312. Springer.

Nagib, H., Christophorou, C., Ruedi, J. D., Monkewitz, P., Osterlund, J., Gravante, S., Chauhan, K. and Pelivan, I. 2004 Can we ever rely on results from wall-bounded turbulent flows without direct measurements of wall shear stress? In *24th AIAA aerodynamic measurement technology and ground testing conference*, p. 2392.

Quadrio, M. 2011 Drag reduction in turbulent boundary layers by in-plane wall motion. *Philos. Trans. A Math. Phys. Eng. Sci.* **369** (1940), 1428–1442.

Romero, S. K., Zimmerman, S. J., Philip, J. and Klewicki, J. C. 2022 Stress equation based scaling framework for adverse pressure gradient turbulent boundary layers. *Int. J. Heat Fluid Flow* **93**, 108885.

Schlatter, P. and Örlü, R. 2010 Assessment of direct numerical simulation data of turbulent boundary layers. *J. Fluid Mech.* **659**, 116–126.

Sillero, J. A., Jiménez, J. and Moser, R. D. 2013 One-point statistics for turbulent wall-bounded flows at reynolds numbers up to δ+ 2000. *Phys. Fluids* **25** (10).